Journal of Climate Change
ISSN 2395-7611 Volume 12 (2026) No. 1. pp. 15–31

https://doi.org/10.70917/jcc-2026-001
Article

Intraseasonal Variability and Synergistic Effects on Extreme Temperature Variations in Eastern China during the 2023–2024 Winter

Guangxin He [1,2], Junru Li [1,2], Boqi Liu [3] , Jingjing Duan [4,*] and Jingjia Luo [1]

[1] State Key Laboratory of Climate System Prediction and Risk Management (CPRM)/CIC-FEMD/KLME/ILCEC, Nanjing University of Information Science and Technology, Nanjing 210044, China
[2] Nanchang Meteorological Bureau, Nanchang 330000, China
[3] State Key Laboratory of Severe Weather Meteorological Science and Technology, Chinese Academy of Meteorological Sciences, Beijing 100081, China
[4] Ningbo Meteorological Bureau of Zhejiang Province, Ningbo 315012, China
* Correspondence author: duanduan1110@163.com

Abstract: In the context of global warming, abrupt transitions between extreme temperature states (extreme temperature variability events) pose severe threats to both ecosystems and socioeconomic systems. However, previous studies have primarily focused on the regulatory effects of atmospheric intraseasonal oscillation (ISO) on extreme temperatures from the perspective of a single scale, leaving the synergistic driving mechanisms of multi-scale ISO on extreme temperature variability poorly understood. This study investigates the synergistic influence mechanisms of 10–30-day and 30–60-day ISO on extreme temperature variability events in eastern China. Utilizing ERA5 reanalysis data from 1979 to 2024, the record-breaking extreme winter of 2023–2024 is employed as a representative case study to systematically elucidate these mechanisms. The results indicate that the winter of 2023–2024 was marked by a record-high surface air temperature variance, accompanied by two prominent extreme temperature variation processes. Wavelet and empirical orthogonal function (EOF) analyses reveal that both ISOs were anomalously strong during this winter and exhibited significant positive correlations with temperature variance, with the 10–30-day ISO playing a more dominant role. Phase evolution analysis demonstrates that phase-locking between the leading 10–30-day modes precedes extreme temperature events by approximately 5 days, whereas the 30–60-day ISO modulates the monthly-scale persistent warm or cold backgrounds. Dynamic diagnosis shows that the ISO-related wave activity flux drives the evolution of key circulation systems, such as the Ural blocking high and the East Asian trough, thereby governing the abrupt temperature reversals. Thermodynamic budget analysis highlights the dominant role of diabatic heating, particularly in the northern key region, where its 10–30-day component is crucial for rapid temperature reversals. Critically, a synergistic effect significantly amplifies the intensity and frequency of extreme temperature variations when both ISOs are in positive phases concurrently. This study advances the understanding of the multi-scale dynamical mechanisms underlying extreme temperature variability and provides a scientific foundation for the extended-range forecasting of such events. Moreover, the findings offer critical insights for enhancing regional climate resilience and informing risk mitigation strategies for major urban clusters in eastern China.

Keywords: Extreme Temperature Variations; Intraseasonal Oscillation; Eastern China; Synergistic Effect

1. Introduction

According to the authoritative assessment by the Intergovernmental Panel on Climate Change (Legg, 2021), the frequency and severity of extreme weather and climate events are being significantly increased

by global climate change. A defining characteristic of these events is that their intensity or duration exceeds upper or lower threshold limits relative to historical baseline conditions (Alexander et al., 2006; Donat et al., 2013; Frich et al., 2002; Sheridan et al., 2018). Consequently, the impacts on natural ecosystems and human societies are often far exceeded by those resulting from fluctuations within the normal range of weather variability. The effects are multifaceted and highly destructive: for example, heatwaves are directly triggered by extreme high temperatures, leading to an increase in heat-related illnesses and fatalities (Vandentorren et al., 2004); large-scale damage to forest trees and widespread failure of critical infrastructure, such as power grids, are caused by intense winter storms (Kloster et al., 2019); and catastrophic floods not only destroy infrastructure and private property but also threaten water security and degrade the water quality and ecology of rivers and lakes through increased nutrient loads (Doocy et al., 2013; Wilson et al., 2019). Collectively, severe challenges are posed to public safety, economic stability, and ecological balance by these events. Against the backdrop of global warming, record-breaking extreme events are occurring with increasing frequency (Cohen et al., 2014; Fischer et al., 2015; Ma et al., 2019; Shepherd, 2016; Wallace et al., 2014), and growing attention is being garnered from the scientific community, policymakers, and risk management sectors. The accurate forecasting, effective response to, and fundamental mitigation of climate change to reduce the risks of future extreme events have become an urgent and pressing challenge that is faced globally.

Although significant progress has been made in extreme event research, most studies remain focused on single types of extreme events, for example, analyzing the formation mechanisms of heatwaves or cold spells in isolation (Smith et al., 2020). This perspective often fails to capture the dynamic linkages between extreme events and their compound impacts, which arise from successive occurrences. In fact, extreme events are often manifested in 'compound' forms, where two or more events occur simultaneously or in rapid succession (Zscheischler et al., 2017). Among these, a particularly distinctive type of compound event is constituted by an abrupt reversal from one extreme weather state to its opposite—such as rapid and severe oscillations in temperature (Ma et al., 2021), precipitation (Tan et al., 2023; Zhang et al., 2023), and atmospheric circulation (Francis, Jennifer A. et al., 2022; Francis, Jennifer A et al., 2023)—which is commonly referred to as 'Weather Whiplash' in both media and academic circles. This study is focused specifically on Extreme Temperature Variations, which refer to the rapid transition between extreme warmth and extreme cold over a short period.

Extreme temperature variation events have been frequently observed worldwide, exerting destructive impacts on human society and the natural environment (Laucelli et al., 2014; Marino et al., 2011; Vicedo-Cabrera et al., 2016; Zou et al., 2017). Notable events have been documented globally. For instance, in March 2012, a temperature plunge from approximately 10°C above normal to 5°C below normal was experienced in North America in less than a week, inducing a "false spring" where crops bloomed early only to be damaged by a subsequent cold snap(Ault et al., 2013). In September 2020, an abrupt shift from a severe heatwave to a blizzard was observed in the Rocky Mountain region of North America within 24 hours, with temperatures dropping more than 20°C, which triggered widespread power outages, property damage, and disruptions to daily life (Russell et al., 2024; Whitehurst et al., 2020). Similarly, in April 2021, Europe experienced a significant extreme temperature variation, where a shift from warm to cold conditions resulted in widespread frost damage to crops (Blunden et al., 2022). In mid-December 2023, a pronounced warm-to-cold shift was witnessed across central and eastern China. Notably, the Southern Suburban Observatory in Beijing recorded the longest continuous period of sub-zero temperatures since 1951, lasting 300 hours (Ye et al., 2025). This event, which was accompanied by heavy snowfall, led to a severe accident on the Beijing Subway Changping Line, resulting in more than 500 hospitalizations. These high-impact disasters underscore the urgent need to establish a comprehensive understanding of the mechanisms governing rapid transitions between extreme temperature states. Currently, research in this field remains notably underdeveloped, with studies on extreme temperature variation events in China being particularly scarce.

Research has shown that in mid- to high-latitude regions, near-surface air temperature variability is significantly regulated by atmospheric intraseasonal oscillation (ISO), which exerts a substantial influence during both winter and summer in the Northern Hemisphere. During winter, ISO is primarily characterized by a distinct southeastward propagation, with its associated temperature anomalies being closely coupled with geopotential height anomalies in the upper troposphere. This propagation is primarily driven by the advection of temperature anomalies by the mean wind field and by Rossby wave energy dispersion originating from the high-latitude regions of Europe and the Atlantic (Yang et al., 2016). Furthermore, a clear modulation of surface air temperature (SAT) in China by ISO activity has been established: statistical analyses indicate that the probability of extreme high-temperature events increases significantly during ISO phases 3–5, whereas extreme low-temperature events occur more frequently during phases 6–1 (Yang et al., 2019). Additionally, the modulating effect of the ISO oscillation period on temperature anomalies must be considered, as the impact of ISO on extreme

temperature events is found to vary with different oscillation periods(Yang et al., 2014). Therefore, investigating the synergistic influence of ISO on temperature variations across different oscillation periods is of significant importance.

However, the aforementioned studies have primarily concentrated on the regulatory effects of a single ISO period on the probability of occurrence of extreme temperature events, and have not systematically explored how multiple ISO periods synergistically regulate the process of abrupt temperature transitions between cold and warm extremes. Indeed, the atmospheric intraseasonal oscillation (ISO) is a multi-scale coupled system. Within this system, the 10–30-day and 30–60-day periods may jointly influence temperature variability through different dynamical pathways, and through their synergistic effects, the intensity and frequency of extreme temperature variability could be significantly amplified. Currently, research on the synergistic mechanisms of multi-scale ISO underlying winter extreme temperature variability events in eastern China remains extremely limited. Eastern China is a region particularly sensitive to climate change and characterized by extremely high population density. Consequently, its southern regions frequently experience abrupt temperature fluctuations during winter. Therefore, this study employs the ERA5 reanalysis data from 1979 to 2024 to investigate the mechanisms responsible for winter extreme temperature variability events across eastern China, as well as the influence of synergistic effects among different ISO periods on these temperature fluctuations.

2. Data

The data used in this study were obtained from the ERA5 reanalysis dataset, produced by the European Centre for Medium-Range Weather Forecasts (ECMWF). As the fifth-generation ECMWF atmospheric reanalysis, ERA5 provides a comprehensive record of global meteorological variables at a high temporal and spatial resolution. For this investigation, the global daily mean data were employed, encompassing variables such as two-meter temperature, precipitation, three-dimensional temperature, zonal and meridional wind, vertical velocity, and geopotential height. The dataset covers the period from 1979 to 13 March 2024, with a horizontal spatial resolution of 1° × 1°. Except for surface variables, the data are provided on 37 atmospheric pressure levels. All data processing and formatting were performed using the Climate Data Operators (CDO) software, and the outputs were standardized in compliance with the CF-1.6 convention.

3. Method

3.1. Definition of Extreme Temperature Variation

Extreme temperature variation refers to a phenomenon in which a persistent temperature regime lasting from several days to weeks abruptly transitions to the opposite persistent state, often concurrently breaking extreme temperature records. Building upon previous research (Ma et al., 2021), this study defines a "negative extreme temperature change event" as a transition from an extreme warm period to an extreme cold period occurring within a 3-to-7-day time window. Correspondingly, a "positive extreme temperature change event" is defined as a transition from an extreme cold period to an extreme warm period. A warm period is defined as a period of more than three consecutive days during which the regional average daily surface air temperature anomaly remains positive. Furthermore, this period must contain at least one "warm day," during which the surface air temperature anomaly over the study region exceeds +1σ, where σ represents the standard deviation of the daily surface air temperature anomaly (approximately 2.94 K). The definition of a cold period is analogous: it requires a period of more than three consecutive days with a negative regional average daily surface air temperature anomaly, and this period must contain at least one "cold day," during which the surface air temperature anomaly falls below -1σ.

3.2. Wavelet Analysis and Significance Testing

To identify the dominant oscillation periods in eastern China's two-meter temperature anomalies during the study winter, the Morlet wavelet transform was applied to perform wavelet and power spectrum analyses. To extract the 10–30-day and 30–60-day intraseasonal oscillation components, a Lanczos band-pass filter (Duchon, 1979) was applied to perform time-domain filtering on the daily meteorological fields. A filter length of 121 days was selected (i.e., M = 60, utilizing data from 60 days before to 60 days after each time point for convolution) to achieve a sharp frequency response, thereby enabling accurate separation of the target intraseasonal signals. The filter weight coefficients (w_k) were generated using the Lanczos window function, the specific formula for which is provided in Duchon (1979). To mitigate boundary effects, the original time series was extended by 60 days at both ends using the 1979–2024 climatology for interpolation, and the target period was subsequently extracted from the

filtered data.

When conducting correlation analysis and trend tests, climatic time series must be handled with care, as they typically exhibit significant autocorrelation. This autocorrelation can lead to an overestimation of degrees of freedom in traditional t-tests, thereby increasing the probability of Type I errors. To address this issue, the method proposed by Bretherton et al. (1999) was employed to estimate the effective degrees of freedom (N_eff) of the time series. Subsequently, significance testing for the Pearson correlation coefficients was performed using these effective degrees of freedom. To assess the significance of linear trends, a t-test based on effective degrees of freedom was also applied. This approach ensures that the influence of serial correlation on the trend significance assessment is effectively eliminated (Bretherton et al., 1999; Huang, 2004; Wei, 2007; Wu et al., 2005).

3.3. Anomalous temperature tendency equation

To investigate the key processes governing the propagation of intraseasonal temperature anomalies, a temperature budget diagnosis was conducted at selected pressure levels. The anomalous temperature tendency equation is expressed as follows(Holton et al., 2013):

$$\left(\frac{\partial T}{\partial t}\right)' = -\left(u\frac{\partial T}{\partial x}\right)' - \left(v\frac{\partial T}{\partial y}\right)' + (\omega\sigma)' + \left(\frac{\dot{Q}}{C_p}\right)' \quad (1)$$

$$\sigma = \frac{\alpha}{C_p} - \frac{\partial T}{\partial p} \quad (2)$$

In the formula, α is the specific volume of air; Cp is the specific heat of air, and $\dot{Q}$ represents the non-adiabatic heating rate. Other symbols follow meteorological conventions.

3.4. T-N wave activity flux

The T-N wave activity flux can be used to describe the propagation and accumulation of wave energy, with the two-dimensional horizontal expression as follows(Takaya et al., 2001):

$$W = \frac{p}{2|U|}\begin{bmatrix}\bar{u}(\psi_x'^2 - \psi'\psi'_{xx}) + \bar{v}(\psi'_x\psi'_y - \psi'\psi'_{xy}) \\ \bar{u}(\psi'_x\psi'_y - \psi'\psi'_{xy}) + \bar{v}(\psi_y'^2 - \psi'\psi'_{yy})\end{bmatrix} \quad (3)$$

where $\bar{u}$ and $\bar{v}$ represent the climatological states of zonal wind and meridional wind, ψ' represents the perturbation of the stream function relative to the climatological state, with subscripts x and y indicating the zonal and meridional partial derivatives of the physical quantities, respectively, p is the normalized pressure value (p = Pressure/1000 hPa), and |U| is the absolute value of the horizontal wind speed.

3.5. Definition of synergy

To quantitatively characterize the combined influence of two climatic factors (such as the variability of the Siberian High and the East Asian Trough) on a physical variable y (e.g., temperature variability or circulation-related variables), the following definitions were adopted in this study to distinguish between synergistic and antagonistic effects(Wang et al., 2024): Herein, the response of y when only event A occurs is denoted by y_1, the response when only event B occurs is denoted by y_2, and the response when both events occur simultaneously is denoted by y_{12}. If $|y_{12}| > \max(|y_1|, |y_2|)$, the combined influence is defined as a synergistic effect on y; if $|y_{12}| < \min(|y_1|, |y_2|)$, their combined influence is defined as an antagonistic effect; otherwise, the combined effect is classified as either a linear superposition or a negligible nonlinear interaction.

4. Experiments and Analysis

4.1. Context of Extreme Temperature Variation

Variability metrics have been utilized in previous studies to assess abrupt weather change events (Francis, Jennifer A. et al., 2022). In this study, the variance of winter (December–January–February) 2-meter air temperature anomalies is adopted as the criterion for identifying extreme temperature variation events, where a larger variance indicates greater intensity of temperature fluctuations and a higher probability of such events. Based on the climatological mean and variance of winter 2-meter air temperature anomalies (Figure 1a), the region characterized by high variance values (105°–135°E, 18°–54°N) was selected as the study area representing Eastern China.

To identify extreme years for detailed analysis, the long-term climatic background of temperature variability was examined. The interannual variations of winter 2-meter air temperature variance over East Asia from 1979 to 2024 are presented in Figure 1b. The alternation between red bars (above the mean) and blue bars (below the mean) reflects distinct phases of enhanced and weakened winter temperature variability over Eastern China. Notably, since 2015, the frequency of red bars has increased

significantly, and the temperature variance exhibits an overall increasing trend, suggesting that extreme temperature events may be increasing in both frequency and intensity. The variance of temperature anomalies in the winter of 2023–2024 was observed to be significantly higher than the historical average (green dashed line), attaining its maximum value for the entire study period. This indicates that the intensity of extreme temperature variability during this season was the strongest recorded. This scenario, therefore, provides an ideal "natural laboratory" in which to examine how multiple ISO periods synergistically drive abrupt temperature transitions between cold and warm extremes.

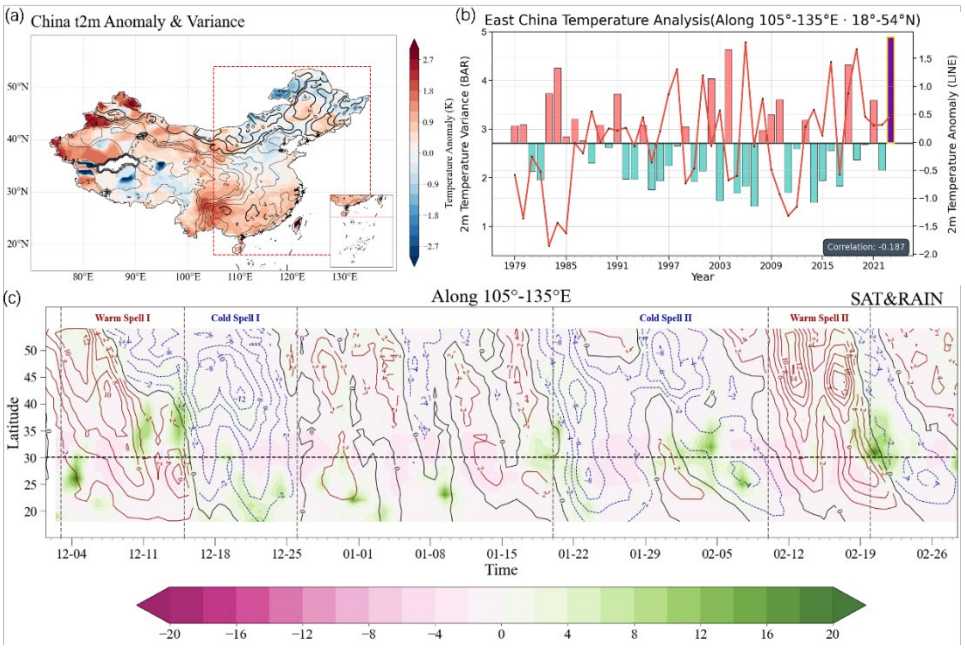

Figure 1. (a) Climatological mean of winter 2-meter air temperature anomalies (shading, units: K) and their variance (contours, units: K) over China for the period 1994–2023. (b) Interannual time series of regional winter temperature variance (bar plot, units: K; red/blue bars indicate values above/below the mean denoted by the green dashed line) and regional winter mean temperature anomaly (line plot, units: K) during 1979–2023. (c) Winter temperature anomaly (contours, units: K; solid red lines for positive values, solid black line for zero, dashed blue lines for negative values) and precipitation anomaly (shading, units: mm) over the study region for the winter of 2023–2024.

For this specific winter, surface air temperature (SAT) and precipitation anomalies were extracted for detailed analysis. Within the longitudinal band of 105°–135°E, pronounced anomalous fluctuations in SAT are evident, as shown in Figure 1c. Temperature changes were exceptionally drastic during four prominent events (Warm Spell I, Cold Spell I, Cold Spell II, Warm Spell II), highlighting the extreme variation characteristics of this season. The SAT anomaly contours reveal a distinct double-peak structure. Two cold-air outbreaks occurred in mid-to-late December and early February, respectively. During these events, regional SAT anomalies were significantly negative, with minimum values below -10 K, indicating frequent occurrences of extreme cold. Pronounced positive SAT anomalies preceded and followed these two cold events, forming an abrupt "cold-warm-cold-warm" reversal pattern and constituting two sets of extreme temperature variation processes. Furthermore, precipitation anomalies were primarily distributed between the warm and cold SAT anomalies, implying that the abrupt temperature transitions were accompanied by precipitation, which may have further intensified surface cooling through rainfall-radiative feedback mechanisms.

The wavelet spectrum and global spectrum of 2-meter air temperature anomalies over eastern China during the winter of 2023–2024 are presented in Figure 2a. The wavelet spectrum clearly reveals the variability of temperature anomalies across different time scales, with significant high-energy centers (red and yellow areas) concentrated in the 10–30-day and 30–60-day bands. This indicates a distinct dual-period oscillation of temperature anomalies during this winter, suggesting that these two bands represent the dominant modes of variability. The global spectrum further confirms the significance of these two bands, with both the 10–30-day and 30–60-day cycles exceeding the 95% confidence level (red dashed line), indicating that the associated temperature anomalies are statistically significant.

Figure 2b correspondingly displays the interannual variation of intensity anomalies for the two extracted ISO bands (10–30-day and 30–60-day) derived from the analysis in Figure 2a. Notably, during

the winter of 2023–2024, the intensity anomalies for both ISO bands reached their maximum values in the entire record and were significantly higher than the historical average. The occurrence of such anomalously high intensities is identified as an important driving factor behind the extreme temperature variation events of that winter. Furthermore, the intensity anomaly of the 10–30-day ISO band has exhibited a gradual increasing trend in recent years (particularly after 2015). This trend aligns with the increasing temperature variance, thereby providing further support for the hypothesis of intensified temperature variability under climate change.

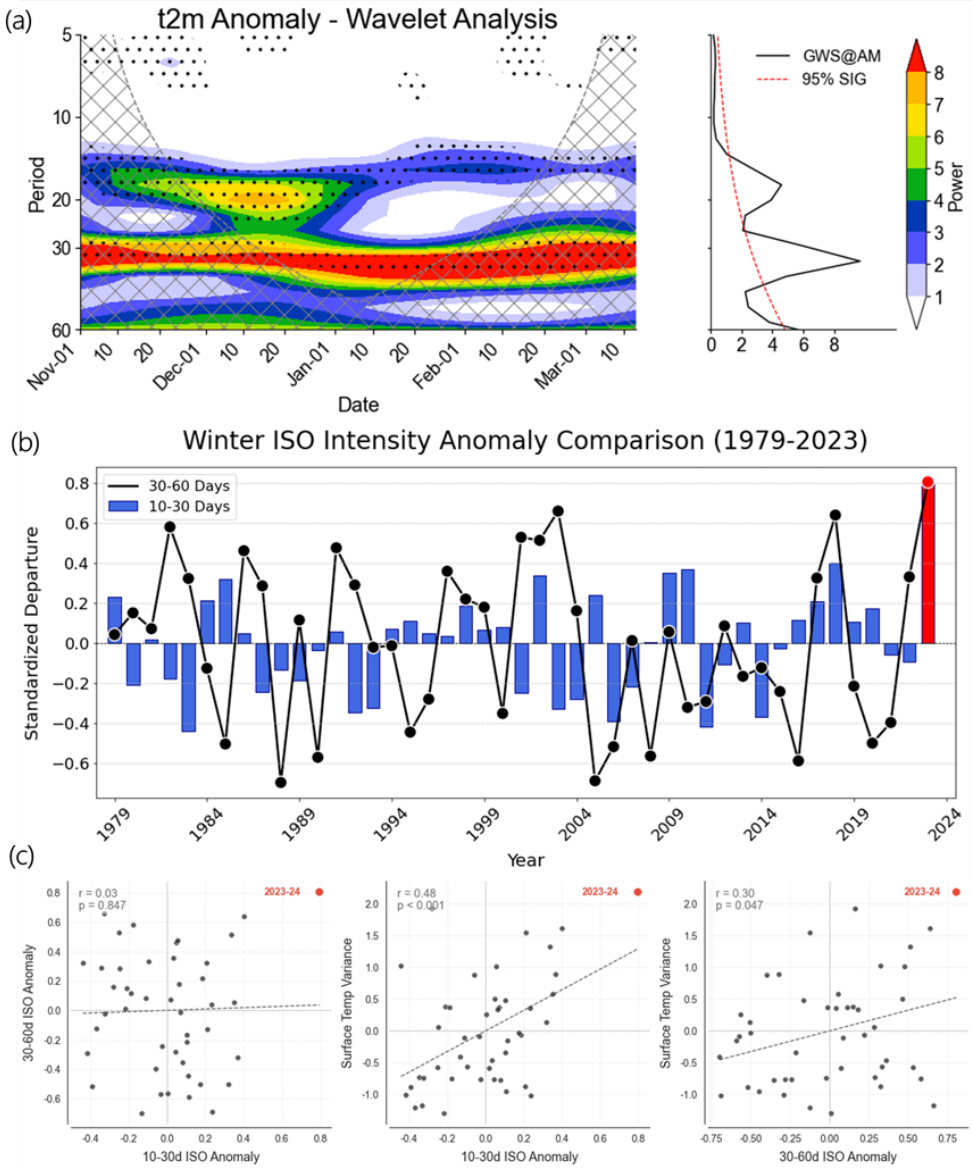

Figure 2. (a) Wavelet spectrum of winter 2-meter air temperature anomalies over eastern China in 2023-2024 (stippled areas denote regions passing the 95% confidence level significance test) and the corresponding global wavelet spectrum (solid black line indicates the power spectrum of temperature anomalies; red dashed line marks the 95% significance level). (b) Interannual variations of 10-30-day ISO intensity anomalies (bar plot, red/blue bars indicating values above/below zero) and 30-60-day ISO intensity anomalies (line plot with solid black line, red/blue markers indicating values above/below zero) over eastern China during winter 1979-2024. (c) Scatter plots of 10-30-day versus 30-60-day ISO intensity anomalies and their relationships with t2m variance (dashed lines represent linear regression fits, The correlation coefficient r and the p-value adjusted based on effective degrees of freedom are annotated in the upper left corner of the figure, with red dots indicating the study years) for winter 1979-2024.

To examine the relationships between the two ISO band intensities and their association with surface

air temperature variance, scatter plots were constructed (Figure 2c). Each scatter point represents one winter, with the color gradient indicating the temporal evolution from 1979 (blue) to 2023 (yellow). In the scatter plot depicting the relationship between the 10–30-day and 30–60-day ISO intensity anomalies, the data point for the 2023–2024 winter is located in the upper-right quadrant of the scatter cloud. No other data points are observed in this quadrant, indicating that both ISO intensities during that winter were significantly higher than the historical average. This synergistic effect of high-intensity ISOs is identified as a key mechanism driving the extreme temperature variation events of that winter. Furthermore, a gradual temporal shift of the combined ISO intensity toward higher values is observed, which may reflect a modulating influence of climate change on intraseasonal oscillations.

A scatter plot of the intensity anomalies for the two ISO bands against surface air temperature variance was constructed. A significant positive correlation was found between the 10–30-day ISO intensity anomaly and surface air temperature variance ($r = 0.48$, $p < 0.001$, adjusted for effective degrees of freedom). This result indicates that enhanced activity at this intraseasonal scale may significantly intensify winter temperature fluctuations in eastern China, thereby playing a key role in regulating winter temperature variability. This finding is also corroborated by the results of the time series comparison discussed above. A positive correlation was also observed between the 30–60-day ISO intensity anomaly and temperature variance ($r = 0.30$, adjusted $p = 0.047$). This correlation attains the conventional significance level ($p < 0.05$), suggesting that the 30–60-day ISO also contributes to anomalous variations in winter surface air temperature, albeit with a weaker influence than that of the 10–30-day ISO.

4.2. Influence of Different ISO Scales on Temperature Variations

4.2.1. Analysis of the 10–30-day ISO

The first EOF mode (EOF1, the explained variance is 13.27%; Figure 3a) represents the typical spatial pattern during the mature phase of extreme temperature anomalies. This mode is characterized by extensive and structurally consistent anomaly patterns of the same sign across the mid-to-high latitudes of Eurasia. The second mode (EOF2, the explained variance is 20.02%.; Figure 3b) exhibits a spatial structure analogous to that of EOF1; however, its anomaly center is shifted southeastward. These spatial configurations suggest that EOF1 corresponds to the canonical configuration of extreme temperature anomalies during their mature phase. This pattern is likely associated with the establishment and maintenance of blocking highs or displacements of the polar vortex. Furthermore, the relative displacement of the anomaly centers between EOF1 and EOF2 elucidates a key characteristic of ISO signal propagation from the northwest to the southeast. Specifically, it reflects the development of anomalous energy from a key source region near the Kara Sea toward the downstream region of eastern China.

The evolution of the principal component (PC) time series (Figure 3c) clearly demonstrates a direct linkage between the phase evolution of the ISO and the occurrence of extreme temperature events. For the 2023–2024 winter case, it is observed that when the peak of PC2 (orange line) successively follows the peak of PC1 (blue line) within the time windows of the four specific temperature events, the actual temperature anomaly (green line) exhibits correspondingly large amplitudes, thereby triggering a significant extreme temperature event. This finding indicates that the specific phase-locking between PC1 and PC2 serves as an important dynamical mechanism leading to the occurrence of extreme temperature events.

Statistical evidence supporting this relationship is provided by the lead-lag correlation analysis shown in Figure 3d. The results indicate that PC2 leads PC1 by approximately 5 days, with the correlation coefficient being statistically significant ($p < 0.05$). This lead-lag relationship indicates that the phase evolution of the ISO follows a distinct sequence: the atmospheric configuration first corresponds to a "trigger phase" characterized by the EOF1 pattern, and then transitions in an organized manner to a "development phase" characterized by the EOF2 pattern. This finding directly links the abstract ISO modes to the temporal evolution of extreme temperature events.

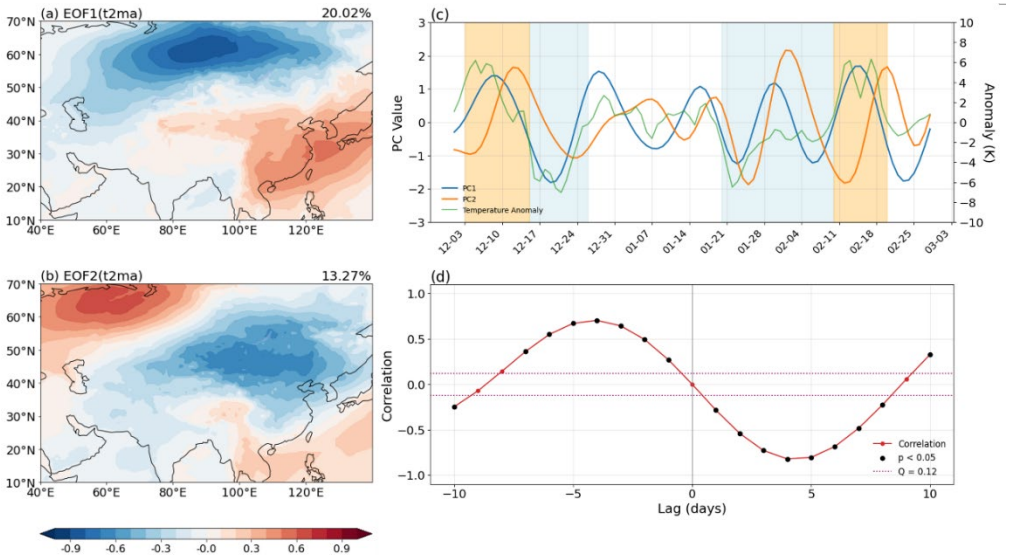

Figure 3. (a) The first EOF mode of 10–30-day filtered winter 2-meter air temperature anomalies for the period 1981–2023(explaining 20.02% of the variance); (b) The second EOF mode (explaining 13.27% of the variance); (c) The 10–30-day filtered PC1 (blue line) and PC2 (orange line) along with temperature anomalies (green line) for the winter of 2023–2024; (d) Lead-lag correlation coefficients between the two principal components (the red dashed line indicates the 0.05 significance level; red dots denote correlations passing the 0.05 significance test; positive (negative) days indicate PC2 leading (lagging) PC1).

The phase evolution sequence of the 10–30-day filtered 2-meter air temperature anomalies and the 850 hPa wind field anomalies during the winter of 2023–2024 is illustrated in Figure 4. From phases 1 to 3, negative temperature anomalies prevail over eastern China, concurrent with the development of an anomalous cyclone in the mid–high latitudes and an anomalous anticyclone near the Kara Sea. This circulation pattern favors the southward transport of cold air from the high latitudes. Phase 4 represents a transition period, during which the core of the negative temperature anomalies weakens and shifts southward. As the circulation pattern adjusts from phases 5 to 7, eastern China becomes consistently dominated by positive temperature anomalies that gradually intensify and peak in phase 7. During this period, the anomalous anticyclone moves southward, establishing control over the region. Its western flank generates southerly wind anomalies that facilitate strong warm advection, resulting in significant warming. By phase 8, the anomalous anticyclone weakens and moves eastward, and the primary center of positive temperature anomalies also shifts away from the region, marking the termination of this warm anomaly episode. Concurrently, a new anticyclonic system forms near the Ural Mountains, and the entire Siberian region is dominated by negative temperature anomalies, signaling the impending invasion of a new cold air mass into eastern China.

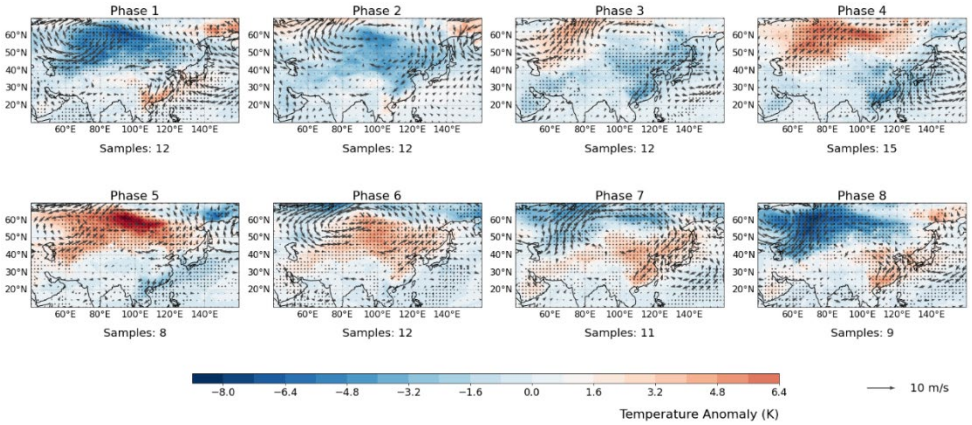

Figure 4. Composite analysis of 10–30-day filtered 2-meter air temperature anomalies (shading, units: K; dotted areas indicate significance at the 95% confidence level) and 850 hPa wind fields (vectors, units: m/s) for the winter of 2023–2024(Sample size is indicated below each phase subplot).

The aforementioned analysis suggests that the evolution of circulation systems is a key driver of extreme temperature variation events in eastern China. This relationship is further investigated from the perspective of wave activity flux.

The phase evolution sequence of the 10–30-day filtered 200 hPa geopotential height anomalies, wind fields, and the Takaya–Nakamura (T-N) wave activity flux during the winter of 2023–2024 is presented in Figure 5. Two distinct west-east oriented wave trains are identified over the Eurasian continent, which are defined as the northern and southern wave trains. The northern wave train propagates from the Kara Sea through West Siberia to Northeast China, whereas the southern wave train propagates eastward from the Middle East to the Bay of Bengal and subsequently reaches South China. These two wave trains represent the primary pathways of energy propagation during the extreme temperature variation events. During phases 1 to 4, the southern wave train is active, with its influence expanding toward eastern China. This pattern indicates that the southern wave train plays a more prominent role in the extreme temperature variation events over this region. During phases 5 to 6, the northern wave train becomes active. In phases 7 to 8, the southern wave train undergoes rapid intensification, while the northern wave train also exhibits considerable intensity in phase 8.

The 200 hPa geopotential height anomaly field exhibits a "+ - +" wave train structure, the spatial distribution of which corresponds well with the quasi-geostrophic perturbation streamfunction. During phases 1 to 4, the negative anomaly center gradually moves eastward from the Caspian Sea region to Northeast China while weakening in intensity, which corresponds to the eastward movement of an upper-level cold vortex. Its association with the activity of the southern wave train constitutes another dynamic factor contributing to the extreme temperature variation in eastern China. It can be concluded that the southern wave train served as the dominant wave train during this extreme temperature variation event.

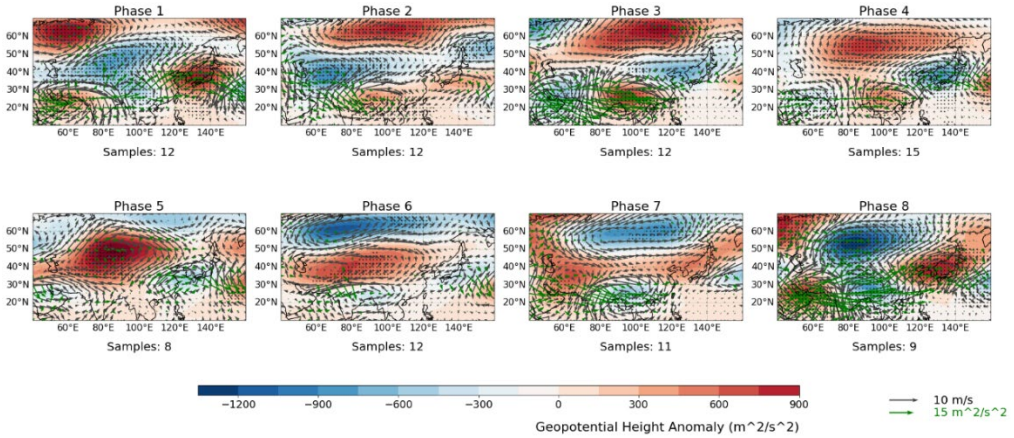

Figure 5. Composite analysis of 10–30-day filtered 200 hPa geopotential height anomalies (shading, units: m²/s²,dotted areas indicate significance at the 95% confidence level), wind fields (black vectors, units: m/s), and Takaya–Nakamura (T-N) wave activity flux (green vectors, units: m²/s²) for the winter of 2023–2024(Sample size is indicated below each phase subplot).

4.2.2. Analysis of the 30–60-day ISO

Following the analytical approach used for the 10–30-day intraseasonal oscillation (ISO), Figures 6(a) and (b) present the first two leading modes of the EOF analysis applied to the 30–60-day filtered temperature anomalies. The first EOF mode (Figure 6a), accounting for 27.11% of the variance, is characterized by a large-scale, spatially coherent pattern of temperature anomalies. Its spatial distribution shares notable similarities and differences with that of the 10–30-day mode (Figure 3a). Specifically, the anomaly centers are typically of greater spatial extent and stronger magnitude, reflecting the macroscopic characteristics of climate variability on longer timescales. This mode accounts for the predominant portion of the total variance and serves as the key background field that governs monthly-scale temperature variations in eastern China during winter. The second EOF mode (Figure 6b), which explains 21.24% of the variance, also exhibits a spatial structure analogous to that of EOF1. Furthermore, the relative displacement of their anomaly centers reveals a key characteristic of ISO propagation from the northwest to the southeast, a feature that exhibits similarities with the 10–30-day mode.

Figure 6c focuses on the winter of 2023–2024, comparing the temporal evolution of the 30–60-day filtered PC1 (blue line) and PC2 (orange line) with the original temperature anomaly series (green line). A phase lag is observed between the PC1 and PC2 trends and the original temperature anomaly series,

and the peak matching is considerably less precise than that observed for the 10–30-day scale. However, the phase transitions of PC1 and PC2 correspond well with the medium-to-long-term winter temperature trends and the major cold and warm phases (e.g., the pronounced cold periods in mid-to-late December and early February). Compared to the high-frequency, rapid oscillations on the 10–30-day scale (Figure 3c), the PC curves for the 30–60-day scale vary more gradually but maintain longer durations in their positive and negative phases. This indicates that oscillations at this scale provide a sustained warm or cold background for extreme temperature variation events, and their phase transitions often mark the initiation or termination of major cold or warm periods.

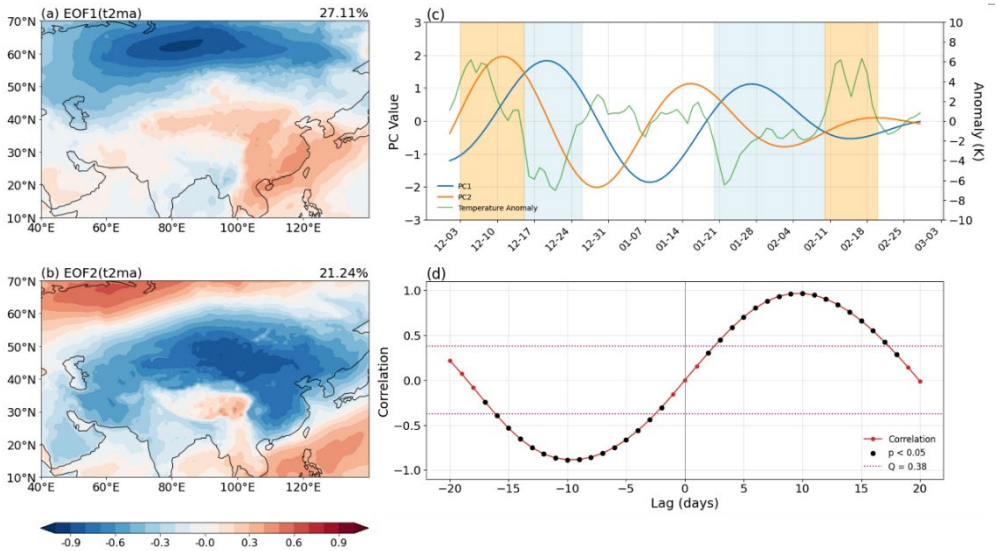

Figure 6. (a) The first EOF mode of 30–60-day filtered winter 2-meter air temperature anomalies for the period 1981–2023 (explaining 27.11% of the variance). (b) The second EOF mode (explaining 21.24% of the variance). (c) Time series of the 30–60-day filtered PC1 (blue line), PC2 (orange line), and the original temperature anomaly (green line) for the winter of 2023–2024; (d) Lead-lag correlation coefficients between the two principal components (red dashed lines indicate the 0.05 significance level; positive (negative) days indicate that PC2 leads (lags) PC1).

To clarify the intrinsic relationship between the two principal components, a lead-lag correlation analysis was performed (Figure 6d). The results reveal a significant negative correlation exceeding the 95% confidence level when PC2 leads PC1 by approximately 10 days. This relationship reveals a regular phase-locking and sequential order between the two leading modes of the 30–60-day ISO, indicating that the development of the spatial pattern represented by PC2 serves as an important precursor to the phase transition of the pattern represented by PC1. This phase-locking relationship, observed across both the 10–30-day and 30–60-day timescales, collectively forms a basis for the predictability of extreme temperature variation events.

The phase evolution sequence of the 30–60-day filtered 2-meter air temperature anomalies and 850 hPa wind field anomalies during the winter of 2023–2024 is displayed in Figure 7. From phases 1 to 4, a strong positive temperature anomaly is observed to propagate persistently from West Siberia toward eastern China, concurrent with the development of a cyclonic circulation anomaly over the region. This circulation pattern facilitated the southeastward propagation of the positive temperature anomaly. Phase 5 represented a critical transition period, during which the core of the positive temperature anomaly weakened and shifted southward. Simultaneously, an anomalous anticyclone initiated development over the Ural Mountains. During phases 6 to 8, the entire eastern China region was dominated by negative temperature anomalies. The cold core intensified progressively throughout these phases, reaching its maximum intensity in phase 8. This cold phase was closely associated with an anomalous anticyclonic system that was stably maintained near the Sea of Japan.

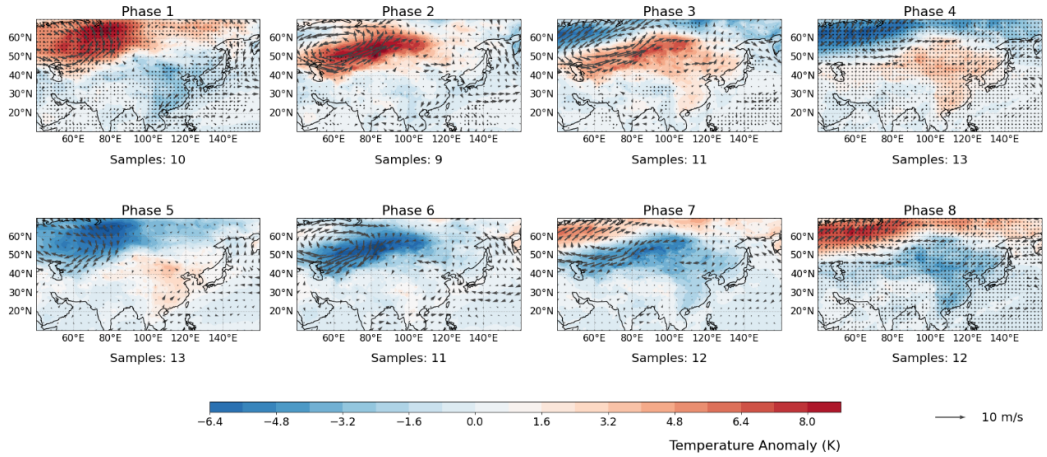

Figure 7. Composite analysis of 30–60-day filtered 2-meter air temperature anomalies (shading, units: K; dotted areas indicate significance at the 95% confidence level) and 850 hPa wind fields (vectors, units: m/s) for the winter of 2023–2024(Sample size is indicated below each phase subplot).

The phase evolution sequence of the 30–60-day filtered 200 hPa geopotential height anomalies, wind fields, and Takaya–Nakamura (T-N) wave activity flux during the winter of 2023–2024 is presented in Figure 8. Characteristics at this scale show some similarities with the 10–30-day scale, as two wave trains are also identified over the Asian region. However, significant differences between the two scales are noted. A distinct wave train is observed across central and eastern Eurasia. This wave train exhibits a northwest-to-southeast energy propagation pathway, traversing Central Asia and the Mongolian Plateau before ultimately influencing eastern China. The wave activity flux intensified substantially and exhibited strong convergence along the East Asian coast during phases 1–3. This pattern reflects the significant influence of this wave train on extreme temperature variation events in the downstream region and identifies it as the primary influential wave train.

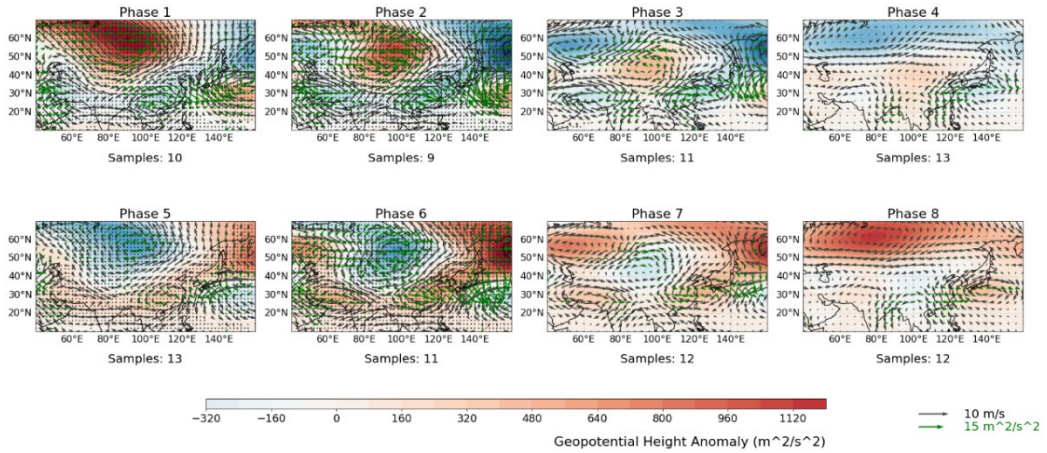

Figure 8. Composite analysis of 30–60-day filtered 200 hPa geopotential height anomalies (shading, units: m^2/s^2, dotted areas indicate significance at the 95% confidence level), wind fields (black vectors, units: m/s), and Takaya–Nakamura (T-N) wave activity flux (green vectors, units: m^2/s^2, only vectors passing the significance test are shown) for the winter of 2023–2024(Sample size is indicated below each phase subplot).

The 200 hPa geopotential height anomalies similarly exhibit a "+ - +" wave train structure. During phases 1–3, a strong positive anomaly center was anchored over West Siberia. Subsequently, this positive anomaly center moved eastward and weakened, whereas during phases 4–6, a negative anomaly center developed and intensified over the Lake Baikal region, corresponding to the activity of an upper-level cold vortex. Finally, the downstream positive anomaly center (i.e., a blocking high) along the East Asian coast became dominant. The convergence of wave activity flux contributed to the deepening of the upstream negative anomaly (cold vortex) and the maintenance of the downstream positive anomaly (blocking high), thereby promoting the formation of a stable dipole circulation pattern. The blocking effect of the downstream high favored the persistence of the cold vortex and confined the cold air to the

key region. In contrast, wave activity flux signals originating from lower latitudes were relatively weak at this scale. Their energy transport to the main wave train was most apparent during phases 4–6, collectively contributing to the establishment of the dipole circulation pattern.

To elucidate the thermodynamic mechanisms governing extreme temperature variations, the spatial distributions of the vertically integrated (1000–300 hPa) terms from the thermodynamic equation over eastern China during the four temperature events are presented in Figure 9. The terms—zonal temperature advection, meridional temperature advection, adiabatic heating, and diabatic heating—are overlaid with 2-meter air temperature anomalies and the horizontal wind field at 850 hPa. This decomposition illustrates the relative contributions of different thermodynamic processes to the temperature anomalies. The largest magnitudes are primarily associated with the meridional temperature advection and diabatic heating terms, with the latter being particularly prominent.

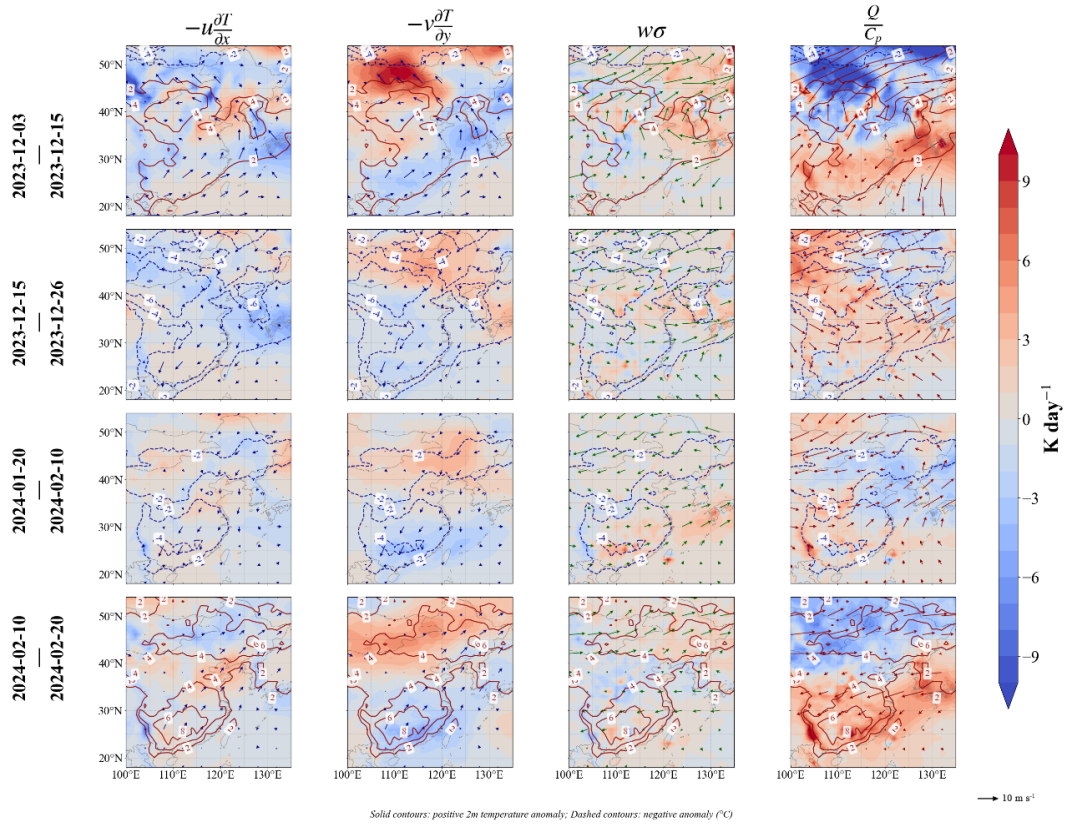

Figure 9. Spatial distribution of the vertical integral (1000–300 hPa) of terms in the thermodynamic equation during the four extreme temperature events in the winter of 2023–2024 over eastern China (shading, units: K/day), along with 2-meter temperature anomalies (contours, units: K, with red solid lines for values greater than 0 and blue dashed lines for values less than 0) and horizontal wind field anomalies (vectors, units: m/s). The temperature advection term is superimposed with the 850 hPa wind field, the adiabatic term is superimposed with the 500 hPa wind field, and the diabatic heating term is superimposed with the 300 hPa wind field.

The temperature advection terms represent the horizontal transport of cold and warm air. The spatial distribution of meridional temperature advection indicates that positive values dominate northern eastern China, whereas negative values prevail in the southern region during these events. In contrast, the diabatic heating term exhibits the largest magnitude among the four terms, which is primarily associated with latent heat release and radiative processes. It displays positive values in the south and negative values in the north during warm spells, whereas this pattern is reversed during cold spells.

A synthesis of both terms indicates that temperature variations over eastern China during the winter of 2023–2024 were predominantly forced by diabatic heating. Furthermore, the analysis reveals the existence of two distinct key regions for temperature changes, located in the north and south. In the northern region, temperature changes are primarily driven by diabatic heating, whereas in the southern region, diabatic heating operates in conjunction with contributions from other terms. Based on the spatial distribution of 2-meter air temperature anomalies (Figure 3), northern and southern key regions were selected to examine the temporal variations of the thermodynamic equation terms and to analyze their

linkages with the Siberian High and the East Asian Trough. The northern key region is defined as 35°–45°N, 110°–120°E, and the southern key region as 22°–30°N, 106°–117°E.

A detailed characterization of the vertically integrated thermodynamic budget terms over the southern and northern key regions in eastern China during the winter of 2023–2024 is provided in Figure 10, from both regional and temporal perspectives. Panels a and b present the time series of the four terms—zonal temperature advection, meridional temperature advection, adiabatic heating, and diabatic heating—for the northern (35°–45°N, 110°–120°E) and southern (22°–30°N, 106°–117°E) key regions, respectively.

In the northern key region, the magnitude of the diabatic heating term is substantially larger than those of the other terms, establishing it as the dominant factor. Furthermore, its peaks correspond closely with those of the local temperature anomaly tendency, providing strong evidence that diabatic heating is the primary driver of temperature variations in this region. In the southern key region, although the absolute magnitudes of all terms are smaller, the diabatic heating term exhibits more pronounced fluctuations during abrupt temperature transitions, reflecting a higher sensitivity to radiative and latent heat processes in this region. indicates that local radiative feedback (such as cloud-mediated feedback) is the primary driver of rapid temperature changes.

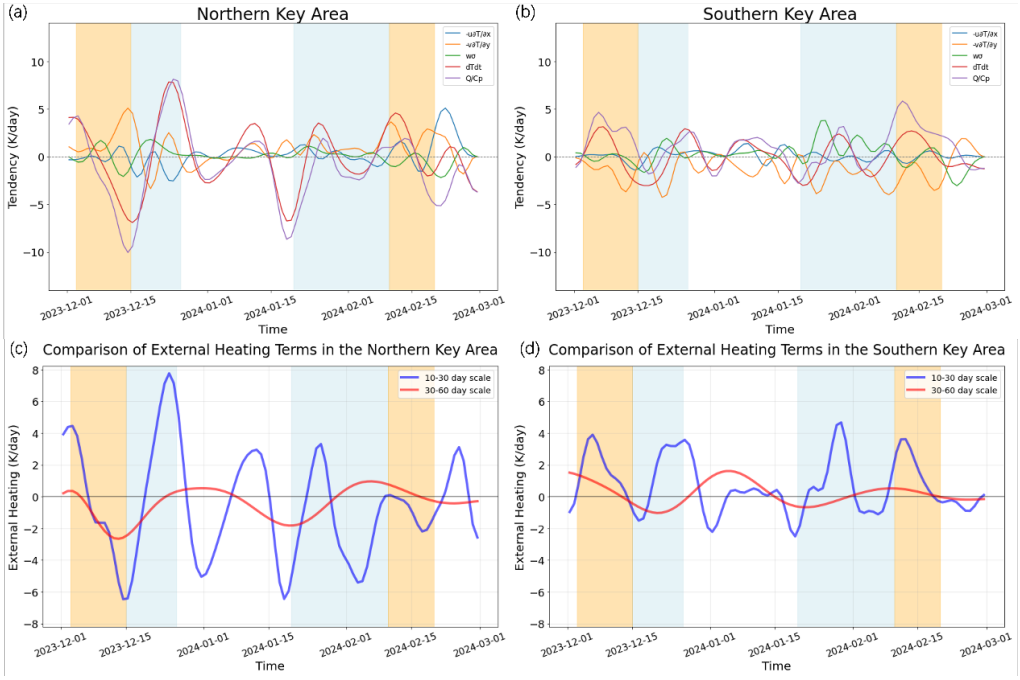

***Figure* 10.** (a) Vertically integrated (1000–300 hPa) terms of the thermodynamic equation over the northern key region (35°–45°N, 110°–120°E) in eastern China during the winter of 2023–2024 (line plot, different colored lines represent different terms in the equation); (b) Vertically integrated (1000–300 hPa) terms of the thermodynamic equation over the southern key region (22°–30°N, 106°–117°E) in eastern China during the winter of 2023–2024 (line plot, different colored lines represent different terms in the equation); (c) Vertically integrated (1000–300 hPa) diabatic heating term at different timescales over the northern key region in eastern China during the winter of 2023–2024 (line plot, blue for 10–30-day bandpass-filtered, red for 30–60-day bandpass-filtered); (d) Vertically integrated (1000–300 hPa) diabatic heating term at different timescales over the southern key region in eastern China during the winter of 2023–2024 (line plot, blue for 10–30-day bandpass-filtered, red for 30–60-day bandpass-filtered).

Panels c and d further decompose the diabatic heating term into its 10–30-day and 30–60-day ISO bandpass-filtered components. In the northern key region, the 30–60-day component exhibits more persistent negative or positive anomalies, which correspond to the establishment and maintenance of prolonged cold or warm backgrounds. In contrast, the 10–30-day component displays high-frequency oscillations that are highly synchronized with rapid temperature reversal events. In the southern key region, diabatic heating components at both scales are closely related to extreme temperature variation events. However, the 10–30-day component exhibits sharper transitions at the turning points, further confirming the crucial role of this ISO timescale in triggering regional extreme temperature variation events.

The evolution characteristics of winter temperature variance over eastern China and its synergistic relationship with the 10–30-day and 30–60-day ISO intensity anomalies are analyzed from a long-term climate perspective (1979–2023) in Figure 11. In Figure 11a, the black line represents the regionally averaged temperature variance series, the gray dashed line indicates the climatological mean, and the red trend line reveals a statistically significant upward trend in the variance since 2015. This trend indicates a continuous enhancement of winter temperature variability under ongoing climate warming. The markers superimposed on the line denote years characterized by positive-phase 10–30-day (red circles) and 30–60-day (blue triangles) ISO intensity anomalies. It is observed that in most high-variance years, the intensity anomalies of both ISOs are in a positive phase, with the winter of 2023–2024 being the most pronounced. This pattern suggests that strong ISO activity is an important driver of enhanced winter temperature variance.

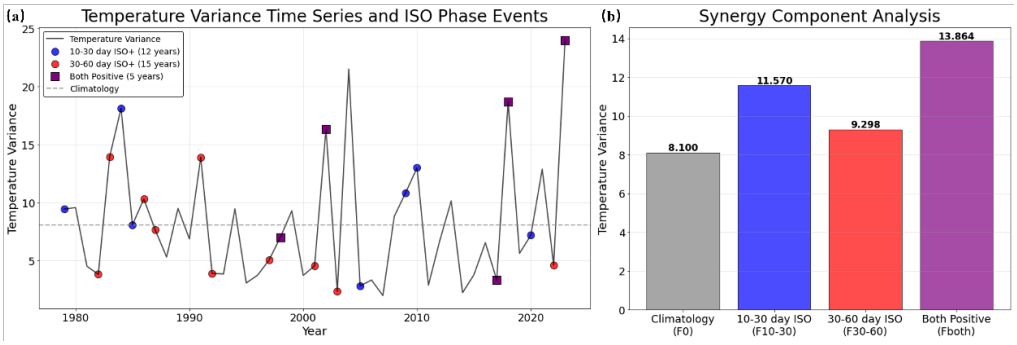

Figure 11. (a) Time series of winter temperature variance in eastern China from 1979 to 2023 (black line). The gray dashed line denotes the climatological mean, and the red line represents the linear trend. Overlaid on this series are markers indicating the positive phases of the 10–30-day and 30–60-day ISO intensity anomalies: blue dots denote the 10–30-day period, red dots denote the 30–60-day period, and purple squares indicate periods when both ISO bands are simultaneously in their positive phases. (b) Analysis of the synergistic effects of the 10–30-day and 30–60-day ISO intensity anomalies. This panel presents a bar chart, where bars of different colors represent the magnitude of temperature variance under different phase combinations. The colors in this panel correspond to those used in (a).

The synergistic influence of the two ISO bands on temperature variance under different phase combinations is further quantified using bar plots in Figure 11b. The temperature variance is 11.570 when only the 10–30-day ISO intensity anomaly is positive, 9.298 when only the 30–60-day ISO is positive, and reaches 13.864 when both are positive simultaneously. Based on the definition of synergistic and antagonistic effects, it is concluded that the two ISO scales exhibit a synergistic effect on temperature variability in eastern China. Furthermore, the temperature variance during co-occurring positive phases is significantly greater than the overall mean variance. This demonstrates that positive ISO phases enhance temperature variance and that their in-phase reinforcement can substantially amplify the magnitude and variability of temperature anomalies, thereby creating a favorable background for the occurrence of extreme temperature variation events. This synergistic mechanism likely stems from the coupling of the two ISO scales in circulation evolution, exemplified by the superposition of upper-level wave trains and the enhanced dispersion of wave energy, which collectively modulate the extremity and variability of winter temperatures in eastern China.

5. Conclusion

Based on ERA5 reanalysis data from 1979 to 2024, this study systematically analyzed the intraseasonal oscillation characteristics and dynamical mechanisms of winter extreme temperature variation events over eastern China, focusing on the synergistic influences of the 10–30-day and 30–60-day ISOs on abrupt transitions between extreme warm and cold spells. The main conclusions are as follows:

1. Pronounced intraseasonal oscillation (ISO) signals are identified in extreme temperature variation events. Eastern China experienced two prominent temperature variation processes during the winter of 2023–2024, during which the temperature variance reached a record high, reflecting an intensifying trend in temperature variability against the backdrop of climate warming.
2. The differentiated regulatory roles of multi-scale ISO in extreme temperature variability are elucidated in this study. The 10–30-day ISO exhibits a stronger correlation with temperature variance,

and its phase evolution precedes extreme temperature events by approximately 5 days, suggesting that it acts as a key dynamic factor in triggering rapid temperature reversals. In contrast, the 30–60-day ISO, by establishing a persistent circulation background, modulates the maintenance and transition of monthly-scale cold and warm phases. Elucidating this differentiation in their respective roles is crucial for understanding the hierarchical influences of multi-scale ISO on extreme temperature variability.

3. The implications of ISO phase evolution for predictability are further clarified in this analysis. A stable lead-lag relationship is observed between PC1 and PC2 of the 10–30-day ISO, with PC2 leading PC1 by approximately 5 days. This relationship suggests that monitoring the evolution of PC2 could provide an early warning of extreme temperature events with a lead time of approximately 5 days. This finding, therefore, offers a potential predictive indicator for extended-range forecasting applications.
4. The evolution of circulation systems and the propagation of wave activity energy are key dynamical pathways through which the ISOs modulate temperature anomalies. On the 10–30-day scale, temperature variations are primarily driven by energy dispersion associated with the northern and southern wave trains originating from the mid-high latitudes, with the southern wave train playing a particularly active role. This drives the phased evolution of circulation systems along the East Asian coast, such as the Ural blocking high and the East Asian trough. On the 30–60-day scale, the dominant feature is a quasi-stationary wave train propagating from northwest to southeast. The convergence of its energy downstream (along the East Asian coast) facilitates the establishment and maintenance of a stable dipole circulation pattern comprising a blocking high and a cold vortex, thereby governing the monthly-scale persistent warm or cold backgrounds and their transitions.
5. Thermodynamic diagnosis reveals that diabatic heating is the dominant process governing temperature variations, particularly in the northern key region. In the southern key region, temperature changes are co-influenced by diabatic heating and temperature advection. Decomposition of the diabatic heating term into the two ISO scales further indicates that the 10–30-day component plays a more prominent role in rapid temperature reversals.
6. A synergistic effect exists between the 10–30-day and 30–60-day ISOs. When both ISOs are in their positive phases simultaneously, the winter temperature variance over eastern China is significantly enhanced, further amplifying the intensity and frequency of extreme temperature variation events.

This study systematically reveals, for the first time, the multi-scale ISO dynamical This study systematically elucidates the multi-scale (synoptic to intraseasonal) dynamical mechanisms and thermodynamic processes governing winter extreme temperature events in eastern China. The critical role of synergistic interactions between two distinct intraseasonal oscillation (ISO) bands in driving extreme temperature variability is underscored. These findings contribute new scientific evidence for understanding the evolution of extreme weather under a warming climate. Furthermore, they offer valuable insights for improving extended-range temperature forecasting and furnish a mechanistic basis for enhancing climate resilience at urban and regional scales. This research is particularly relevant for the densely populated and economically vital urban agglomerations of eastern China, thereby directly informing climate adaptation planning and risk management strategies aimed at mitigating the impacts of intense temperature fluctuations. It is important to note that this study is based primarily on a case analysis of the record-breaking extreme winter of 2023–2024. Although this winter demonstrates a high degree of typicality and representativeness, the generalizability of the findings remains to be validated through composite analyses of multiple high-variance winters. Future work will involve conducting multi-case composite studies based on historical high-variance years to further elucidate the general mechanisms underlying the synergistic regulation of extreme temperature variability over eastern China by the 10–30-day and 30–60-day intraseasonal oscillations (ISOs). Furthermore, this study relies primarily upon the ERA5 reanalysis dataset, which may exhibit inherent biases in the representation of extreme events. Future research will involve integrating multiple reanalysis datasets and in situ observations to validate key thermodynamic processes, thereby further enhancing the robustness of the findings.

Author Contributions

Conceptualization, Junru Li, Boqi Liu and Guangxin He; methodology, Junru Li and Boqi Liu; data curation, Guangxin He and Junru Li; visualization, Junru Li; formal analysis, Junru Li and Boqi Liu; writing—original draft preparation, Junru Li; writing—review and editing, Boqi Liu, Jingjing Duan and Jingjia Luo. All authors have read and agreed to the published version of the manuscript.

Funding
This work was supported by the State Key Laboratory of Climate System Prediction and Risk Management (CPRM) initiative project (Grant No. CPRM-2025¬NUIST-012); the China Meteorological Administration Youth Innovation Team (CMA2023QN10); Sichuan Science and Technology Program（No.2025YFNH0006); Water Conservancy Science and Technology Project of Jiangsu Province (No. 2025017); the funding of Fengyun Application Pioneering Project (FY- APP); the Bohai Rim Regional Meteorological Science and Technology Collaborative Innovation Fund project(QYXM202409).

Conflict of Interest Statement
The authors declare no conflict of interest.

Data Availability Statement
The ERA5 reanalysis dataset is available at https://cds.climate.copernicus.eu.

References

Alexander, L. V., Zhang, X., Peterson, T. C., et al. (2006). Global observed changes in daily climate extremes of temperature and precipitation. *Journal of Geophysical Research: Atmospheres, 111*(D5). doi:10.1029/2005JD006290

Ault, T. R., Henebry, G. M., Beurs, K. M. d., et al. (2013). The False Spring of 2012, Earliest in North American Record. *Eos, Transactions American Geophysical Union, 94*, 181-182. doi:10.1002/2013EO200001

Blunden, J., & Boyer, T. (2022). State of the Climate in 2021. *Bulletin of the American Meteorological Society*. doi:10.1175/2022BAMSStateoftheClimate.1

Bretherton, C. S., Widmann, M., Dymnikov, V. P., et al. (1999). The Effective Number of Spatial Degrees of Freedom of a Time-Varying Field. *Journal of Climate, 12*(7), 1990-2009. doi:10.1175/1520-0442(1999)012<1990:TENOSD>2.0.CO;2

Cohen, J., Screen, J. A., Furtado, J. C., et al. (2014). Recent Arctic amplification and extreme mid-latitude weather. *Nature Geoscience, 7*(9), 627-637. doi:10.1038/ngeo2234

Donat, M., Alexander, L. V., Yang, H., et al. (2013). Updated analyses of temperature and precipitation extreme indices since the beginning of the twentieth century: The HadEX2 dataset. *Journal of Geophysical Research: Atmospheres, 118*(5), 2098-2118. doi:10.1002/jgrd.50150

Doocy, S., Daniels, A., Packer, C., et al. (2013). The human impact of earthquakes: a historical review of events 1980-2009 and systematic literature review. *PLoS currents, 5*, ecurrents. dis. 67bd14fe457f451db450b5433a5438ee5420fb5833. doi:10.1371/currents.dis.67bd14fe457f1db0b5433a8ee20fb833

Duchon, C. E. (1979). Lanczos Filtering in One and Two Dimensions. *J. Appl. Meteor, 18*(8), 1016-1022. doi:10.1175/1520-0450(1979)018<1016:LFIOAT>2.0.CO;2

Fischer, E. M., & Knutti, R. (2015). Anthropogenic contribution to global occurrence of heavy-precipitation and high-temperature extremes. *Nature Climate Change, 5*(6), 560-564. doi:10.1038/nclimate2617

Francis, J. A., Skific, N., Vavrus, S. J., et al. (2022). Measuring "Weather Whiplash" Events in North America: A New Large‐Scale Regime Approach. *Journal of Geophysical Research. Atmospheres, 127*(17). doi:10.1029/2024JD042635

Francis, J. A., Skific, N., & Zobel, Z. (2023). Weather whiplash events in Europe and North Atlantic assessed as continental-scale atmospheric regime shifts. *npj Climate and Atmospheric Science, 6*(1), 216. doi:10.1038/s41612-023-00542-9

Frich, P., Alexander, L. V., Della-Marta, P., et al. (2002). Observed coherent changes in climatic extremes during the second half of the twentieth century. *Climate Research, 19*(3), 193-212. doi:10.3354/cr019193

Holton, J. R., & Hakim, G. J. (2013). *An introduction to dynamic meteorology* (Vol. 88): Academic press.

Huang, J. (2004). Method of Meteorological Statistic Analysis and Forecasting. In: China Meteorological Press: Beijing, China.

Kloster, D. P., Morzillo, A. T., & Volin, J. C. (2019). A national and local media perspective on responsibility for and solutions to storm-related power outages in the northeastern United States. *Environmental Hazards, 18*(3), 228-245. doi:10.1080/17477891.2018.1541782

Laucelli, D., Rajani, B., Kleiner, Y., et al. (2014). Study on relationships between climate-related covariates and pipe bursts using evolutionary-based modelling. *Journal of Hydroinformatics, 16*(4), 743-757. doi:10.2166/hydro.2013.111

Legg, S. (2021). IPCC, 2021: Climate Change 2021: The Physical Science Basis. *Interaction (Melbourne), 49*(4).

Ma, S., & Zhu, C. (2019). Extreme cold wave over East Asia in January 2016: A possible response to the larger internal atmospheric variability induced by Arctic warming. *Journal of Climate, 32*(4), 1203-1216. doi:10.1175/JCLI-D-18-0234.1

Ma, S., & Zhu, C. (2021). Atmospheric circulation regime causing winter temperature whiplash events in North China. *International Journal of Climatology*. doi:10.1002/joc.6706

Marino, G. P., Kaiser, D. P., Gu, L., et al. (2011). Reconstruction of false spring occurrences over the southeastern United States, 1901–2007: an increasing risk of spring freeze damage? *Environmental Research Letters, 6*(2), 024015. doi:10.1088/1748-9326/6/2/024015

Russell, E. N., Loikith, P. C., Ajibade, I., et al. (2024). The meteorology and impacts of the September 2020 Western United States extreme weather event. *Weather and Climate Extremes, 43*, 100647. doi:10.1016/j.wace.2024.100647

Shepherd, T. G. (2016). Effects of a warming Arctic. *Science, 353*(6303), 989-990. doi:10.1126/science.aag0998

Sheridan, S. C., & Lee, C. C. (2018). Temporal trends in absolute and relative extreme temperature events across North America. *Journal of Geophysical Research: Atmospheres, 123*(21), 11,889-811,898. doi:10.1029/2018JD029150

Smith, E. T., & Sheridan, S. C. (2020). Where Do Cold Air Outbreaks Occur, and How Have They Changed Over Time? *Geophysical Research Letters, 47*(13). doi:10.1029/2020GL087422

Takaya, K., & Nakamura, H. (2001). A formulation of a phase-independent wave-activity flux for stationary and migratory quasigeostrophic eddies on a zonally varying basic flow. *Journal of the Atmospheric Sciences, 58*(6), 608-627. doi:10.1175/1520-0469(2001)058<0608:AFOAPI>2.0.CO;2

Tan, X., Wu, X., Huang, Z., et al. (2023). Increasing global precipitation whiplash due to anthropogenic greenhouse gas emissions. *Nature Communications, 14*(1), 2796. doi:10.1038/s41467-023-38510-9

Vandentorren, S., Suzan, F., Medina, S., et al. (2004). Mortality in 13 French cities during the August 2003 heat wave. *American journal of public health, 94*(9), 1518-1520. doi:10.2105/AJPH.94.9.1518

Vicedo-Cabrera, A. M., Forsberg, B., Tobias, A., et al. (2016). Associations of inter-and intraday temperature change with mortality. *American journal of epidemiology, 183*(4), 286-293. doi:10.1093/aje/kwv205

Wallace, J. M., Held, I. M., Thompson, D. W., et al. (2014). Global warming and winter weather. *Science, 343*(6172), 729-730. doi:10.1126/science.343.6172.729

Wang, H., Li, J., Zheng, F., et al. (2024). The synergistic effect of the preceding winter mid-latitude North Atlantic and summer tropical eastern Indian Ocean SST on summer extreme heat events in northern China. *Weather and Climate Extremes, 44*, 100660. doi:10.1016/j.wace.2024.100660

Wei, F. (2007). *Modern Climate Statistical Diagnosis and Prediction Techniques, 2nd ed.*

Whitehurst, L., & Slevin, C. (2020). From heat to snow: Rocky Mountains see 60-degree plunge. *Greenwire*(Sep.9).

Wilson, H. F., Casson, N. J., Glenn, A. J., et al. (2019). Landscape controls on nutrient export during snowmelt and an extreme rainfall runoff event in northern agricultural watersheds. *Journal of environmental quality, 48*(4), 841-849. doi:10.2134/jeq2018.07.0278

Wu, H., & Wu, L. (2005). Diagnosis and Prediction Method of Climate Variability. In: China Meteorological Press: Beijing, China.

Yang, S., & Li, T. (2016). Intraseasonal variability of air temperature over the mid-high latitude Eurasia in boreal winter. *Climate Dynamics, 47*(7), 2155-2175. doi:10.1007/s00382-015-2956-8

Yang, S., Wu, B., zhang, R., et al. (2014). Propagation of Low-Frequency Oscillation over Eurasian Mid–High Latitude in Winter and Its Association with the Eurasian Teleconnection Pattern. *Chinese Journal of Atmospheric Sciences*. doi:10.3878/j.issn.1006-9895.2013.12181.

Yang, S., Zhu, Z., Cui, J., et al. (2019). Regulation of the intraseasonal oscillation over mid-to-high latitude Eurasia on winter surface air temperature over China. *Dynamics of Atmospheres and Oceans, 86*, 63-72. doi:10.1016/j.dynatmoce.2019.03.007

Ye, Y., Qian, C., Dai, A., et al. (2025). Attribution of a record-breaking cold event in the historically warmest year of 2023 and assessing future risks. *npj Climate and Atmospheric Science, 8*(1), 14. doi:10.1038/s41612-024-00886-w

Zhang, B., Wang, S., Zscheischler, J., et al. (2023). Higher exposure of poorer people to emerging weather whiplash in a warmer world. *Geophysical Research Letters, 50*(21), e2023GL105640. doi:10.1029/2023GL105640

Zou, Y., Wang, Y., Zhang, Y., et al. (2017). Arctic sea ice, Eurasia snow, and extreme winter haze in China. *Science Advances, 3*(3), e1602751. doi:10.1126/sciadv.1602751

Zscheischler, J., & Seneviratne, S. I. (2017). Dependence of drivers affects risks associated with compound events. *Science Advances, 3*(6), e1700263. doi:10.1126/sciadv.1700263